Physicochemical and Temporal Characteristics of Individual Atmospheric Aerosol Particles in Urban Seoul during KORUS-AQ Campaign: Insights from Single-Particle Analysis

Hanjin Yoo[1,2], Li Wu[3], Hong Geng[4,+], and Chul-Un Ro[1,2,+]

[1]Department of Chemistry, Inha University, Incheon, 22212, Republic of Korea
[2]Particle Pollution Management Center, Inha University, Incheon, 21999, Republic of Korea
[3]School of Earth Science System, Tianjin University, Tianjin, China
[4]Institute of Environmental Science, Shanxi University, Taiyuan, China

Correspondence to: Chul-Un Ro (curo@inha.ac.kr) and Hong Geng (genghong@sxu.edu.cn)

ABSTRACT

Single-particle analysis was conducted to characterize atmospheric aerosol particles collected at Olympic Park in Seoul, Korea as a part of the Korea-US Air Quality (KORUS-AQ) campaign which was carried out during May-June 2016. The KORUS-AQ campaign aimed to understand the temporal and spatial characteristics of atmospheric pollution on the Korean Peninsula through an international cooperative field study. A total of 8004 individual particles from 52 samples collected between 5/23-6/5, 2016, were investigated using a quantitative electron probe X-ray microanalysis (low-*Z* particle EPMA), resulting in the identification of seven major particle types. These included genuine and reacted mineral dust, sea-spray aerosols, secondary aerosol particles, heavy metal-containing particles, combustion particles, Fe-rich particles, and others (biogenic and humic-like substances (HULIS) particles). Distinctly different relative abundances of individual particle types were observed during five characteristic atmospheric situations, namely (a) a mild haze event influenced by local emissions and air mass stagnation, (b) a typical haze event affected by northwestern air masses with a high proportion of sulfate-containing particles, (c) a haze event with a combined influence of northwestern air masses and local emissions, (d) a clean period with low particulate matter concentrations and a blocking pattern, and (e) an event with an enhanced level of heavy metal-containing particles, with Zn, Mn, Ba, Cu, and Pb being the major species identified. Zn-containing particles were mostly released from local sources such as vehicle exhausts and waste incinerations, while Mn, Ba, and Cu-containing particles were attributed to

metal-alloy plants or mining. The results suggest that the morphology and chemical compositions of atmospheric aerosol particles in urban area vary depending on their size, sources, and reaction or ageing status, and are affected by both local emissions and long-range air masses.

Key Words: KORUS-AQ Campaign; low-*Z* particle EPMA; urban megacity; haze

Introduction

Atmospheric aerosols, originating from various anthropogenic and natural sources, have significant impacts on climate change and human health (**IPCC, 2021**). Anthropogenic emissions greatly influence the composition and behavior of airborne particulate matter (PM) (**Kim et al., 2018b; Chowdhury et al., 2018; Nault et al., 2018**). On the Korean Peninsula, anthropogenic pollutants primarily come from local emissions and long-range transported air masses (**Cho et al., 2021; Park et al., 2020; Choi et al., 2021; Kumar et al., 2021; Nault et al., 2018**). Studies have observed changes in the characteristics of aerosols composed of organic and inorganic compounds influenced by different air mass flows. Secondary organic aerosols (SOAs) are particularly affected by local emissions, while inorganic particles can be influenced by either local emissions or long-range transported pollutants (**Nault et al., 2018; Kim et al., 2018b; Kim et al., 2020; Park et al., 2018; Chen et al., 2017**). Local emissions, including biomass burning, cooking, and traffic exhaust, primarily influence the formation of SOAs in urban areas (**Nault et al., 2018; Park et al., 2018; Kim et al., 2018b**). On the other hand, transboundary transport of pollutants is significantly affected by comprehensive climatic conditions and can lead to air pollution episodes dominated by inorganic components, including sulfate, nitrate, and ammonium (**Kumar et al., 2021; Lee et al., 2019a; Choi et al., 2019**).

East Asia has seen a significant decline in air quality over the past few decades due to increased emissions of gaseous and particulate pollutants as a result of rapid industrial and economic growth. The Korean Peninsula, surrounded by China, Japan, and Russia, exhibits complex aerosol characteristics influenced by a combination of local emissions, surrounding seas, and transboundary long-range transported air masses (**Pochanart et al., 2004; Crawford et al., 2020; Peterson et al., 2019; Ramachandran et al., 2020; Kim et al., 2018a**). To further investigate factors affecting air pollution on the Korean Peninsula, an international cooperative field study, the KORUS-AQ (Korea-US Air Quality) campaign, was conducted during May-June 2016 **(Crawford et al., 2020)**. Through this campaign, the temporal and spatial

characteristics of various gaseous and particulate pollutants on the Korean Peninsula were successfully elucidated, making it an important study in the field of atmospheric science (**Crawford et al., 2020**). In the Korean Peninsula, ammonium was found to be the most sensitive factor affecting $PM_{2.5}$ exposure, followed by NO_x, SO_2, organic carbon (OC), and black carbon (BC) (**Choi et al., 2019**). The presence of anthropogenic ammonium on the Korean Peninsula leads to the formation of ammonium sulfate (AS) and ammonium nitrate (AN) particles (**Kim et al., 2021; Kim et al., 2020**). Regarding the composition of atmospheric PM_1 in Seoul, the most populated metropolitan area in Korea, OC content was found to be the highest, followed by sulfate, nitrate, ammonium, and BC (**Kim et al., 2018b**).

While previous studies have effectively examined the impact of anthropogenic emissions on the formation of submicron particles during the KORUS-AQ campaign, research on supermicron particles remains limited. Aerosol particles in the supermicron fraction, which mainly originate from natural sources like mineral dust and sea-spray aerosols (SSAs), make up a significant proportion of the total aerosol mass (**Andreae and Rosenfeld, 2008; Seinfeld and Pandis, 2006**). Airborne mineral dust particles in East Asia, directly emitted from arid regions of Mongolia and northern China, can undergo physicochemical changes during long-range transportation, for example, through atmospheric reactions with anthropogenic NO_x and SO_2, resulting in the formation of nitrates and sulfates. This leads to alterations in chemical compositions, morphology, size, and radiative forcing capabilities (**Sullivan et al., 2007; Yu et al., 2020; Geng et al., 2014; Heim et al., 2020; Sobanska et al., 2012**). The investigation of the characteristics of supermicron particles, including their particle-particle variability, formation dynamics, and atmospheric fate, is important to gain a comprehensive understanding of the behavior and impact of atmospheric aerosols of natural and anthropogenic origin on air quality and climate change.

This study utilized a quantitative electron probe X-ray microanalysis (EPMA) technique based on scanning electron microscopy coupled with X-ray spectrometry, so-called low-*Z* particle EPMA, to examine the physicochemical characteristics of individual aerosol particles collected at Olympic Park in Seoul, Korea during the KORUS-AQ campaign. Low-*Z* particle EPMA is a powerful single-particle analytical technique for providing information on unique features of individual aerosol particles, including morphology, elemental compositions, and particle-particle variability (**Geng et al., 2009; Geng et al., 2011; Li et al., 2017; Wu et al., 2019**). Differences in these features are attributed to particle sources, formation mechanisms, and atmospheric fate (**Wu et al., 2019; Song et al., 2022**). This article consists of two parts: (1) an examination of the differences in physicochemical characteristics based on

particle species and (2) an analysis of the temporal variations of individual aerosol particles during the KORUS-AQ campaign. The characterization of individual particles, combined with other studies on atmospheric aerosols during the KORUS-AQ period, provides valuable insights into the unique features of urban atmospheric particles.

2. Experiments

2.1 Sampling

Ambient aerosol particles were collected at Olympic Park (37.52˚ N, 127.12˚ E) in Seoul, the capital of South Korea (Fig. S1 in Supporting Information). The Seoul metropolitan area (SMA), with high population density, numerous local emissions, and transboundary long-range transport, provides a suitable location for investigating the complex characteristics of atmospheric aerosols (**Kim et al., 2018b**; **Kim et al., 2020**). A 3-stage cascade Dekati PM10 impactor (Dekati Ltd.) with an aerodynamic cut-off size of 10, 2.5, and 1.0 μm for stages 1-3 at a 10 L min^{-1} flow rate, respectively, was used to collect aerosol particles on Al foils. Each sample set was analyzed for particles collected on stages 2 and 3, corresponding to $PM_{2.5-10}$ and $PM_{1-2.5}$, respectively. A total of 52 sets of samples were collected in the morning and afternoon (9:00 ~ 10:00 and 15:00 ~ 16:00, KST) during May 23 to June 5, 2016. The sampling duration for each stage was controlled to obtain an optimum number of particles without overloading on the Al foils, such as 10-30 minutes for stage 2 and 5-15 minutes for stage 3. 72-hour backward air mass trajectories were generated using the HYSPLIT (Hybrid Single-Particle Lagrangian Integrated Trajectory) model for different receptor heights of 250 m, 500 m, and 1000 m above ground level. The HYSPLIT model is available at the NOAA Air Resources Laboratory's website **(Stein et al., 2015; Rolph et al., 2017;** http://www.arl.noaa.gov/ready/hysplit4.html).

2.2 Determination of individual particle types by low-*Z* particle EPMA

The physicochemical characteristics of individual aerosol particles were examined using a SEM (JEOL JSM-6390) equipped with an Oxford Link SATW ultrathin window EDX detector under the vacuum condition. The resolution of the detector was 133 eV for Mn-Kα X-rays, and X-ray spectra were recorded using INCA Oxford software (Oxford Instruments Analytical Ltd, INCA suite version 4.09). Routine measurement was conducted using an accelerating voltage of 10 kV and beam current of 0.5 nA, while 20 kV and 0.25 nA were used

to confirm heavy metal elements of specific particles. To obtain sufficient X-ray counts for quantitative analysis, a typical measurement time of 15 s was chosen. The net X-ray intensities for the elements were obtained using a non-linear least-squares fitting of the collected spectra using the AXIL program (**Vekemans et al., 1994**). The elemental concentrations of the individual particles were determined from their X-ray intensities using a Monte Carlo calculation combined with reverse successive approximations (**Ro et al., 2001, 2002**). The chemical species of individual aerosol particles were determined based on their size, morphology, and elemental composition. Measurements under the vacuum condition may result in the evaporation of volatile organic components in individual aerosol particles, but these effects are negligible for ambient supermicron aerosols given their general chemical compositions.

3 Results and discussion

3.1 Characteristics and abundances of individual particle types

Individual particles were classified into 13 species based on their morphology and elemental composition, and further categorized into seven major groups based on their sources and/or formation mechanism. These groups are (1) secondary aerosol particles including SOAs and secondary organic and inorganic aerosols (SOIAs), (2) genuine and aged/reacted mineral dust, (3) reacted SSAs, (4) combustion particles, (5) Fe-rich particles, (6) heavy metal-containing particles, and (7) others, including biogenic and humic-like substances (HULIS) particles. More information on the classification can be found in the Supporting Information (Section A and Tables S1). While the internal mixing state of individual aerosol particles can offer valuable insights into the sources and formation mechanisms of ambient aerosols **(Adachi and Buseck., 2013; Li et al., 2021; Zhang et al., 2022)**, this study primarily focuses on the overall physicochemical characteristics and relative abundances of the ambient aerosols due to the extensive number of particles investigated.

3.1.1 Secondary aerosol particles (SOAs and SOIAs)

Secondary aerosol particles, including SOAs and SOIAs, account for 5.6% and 29.3% in the $PM_{2.5\text{-}10}$ and $PM_{1\text{-}2.5}$ fractions, respectively. These particles, likely formed through gas-to-particle conversion, photochemical processes, and the condensation of semi-volatile organic compounds (**Hallquist et al., 2009; Kim et al., 2018a**), are significantly more abundant in the fine $PM_{1\text{-}2.5}$ fraction than in the $PM_{2.5\text{-}10}$ fraction. The morphology, X-ray spectra, and elemental compositions of typical secondary aerosol particles are presented in Fig. 1. SOA particles

appear as dark droplets in their secondary electron image (SEI) and are primarily composed of C and O (>90% in low-*Z* particle EPMA analysis) (Fig. 1a). The spread droplet-like morphology of SOA particles collected on the hydrophilic Al foil suggests that they are likely low-viscous and water-soluble. In contrast, SOIAs, which are mixtures of SOA and inorganic constituents such as NH_4^+, NO_3^-, and/or SO_4^{2-}, exhibit C, N, O, and S in their X-ray spectra and are apparently susceptible to damage by electron beams (Figs. 1b and 1c). The morphology of SOIA particles varies depending on the organic and inorganic contents. Those with high inorganic content appear as bright, crystalline shapes surrounded by a water-soluble footprint (Fig. 1b), while those with a high organic content resemble dark droplets (Fig. 1c). An inset marked with * on Fig. 1c shows a SOIA particle that appears as a core-shell structure, with a SOIA core surrounded by a dark droplet shade mainly containing C and O. The differences in the crystalline morphology of SOIAs indicate that the heterogeneous nucleation and/or crystallization of particles can vary depending on the chemical species present (**Wu et al., 2020**). Furthermore, the significant water-soluble footprint surrounding SOA and SOIA particles indicates that aqueous-phase chemistry is a crucial process in the formation of secondary aerosol particles in the urban area of Seoul. Previous studies have reported that SOA particles in South Korea are primarily influenced by local emissions, while the sources of inorganic components are highly relevant to both local emissions and transboundary long-range transport air masses (**Nault et al., 2018; Kim et al., 2018b; Choi et al., 2019**).

3.1.2 Mineral dust particles

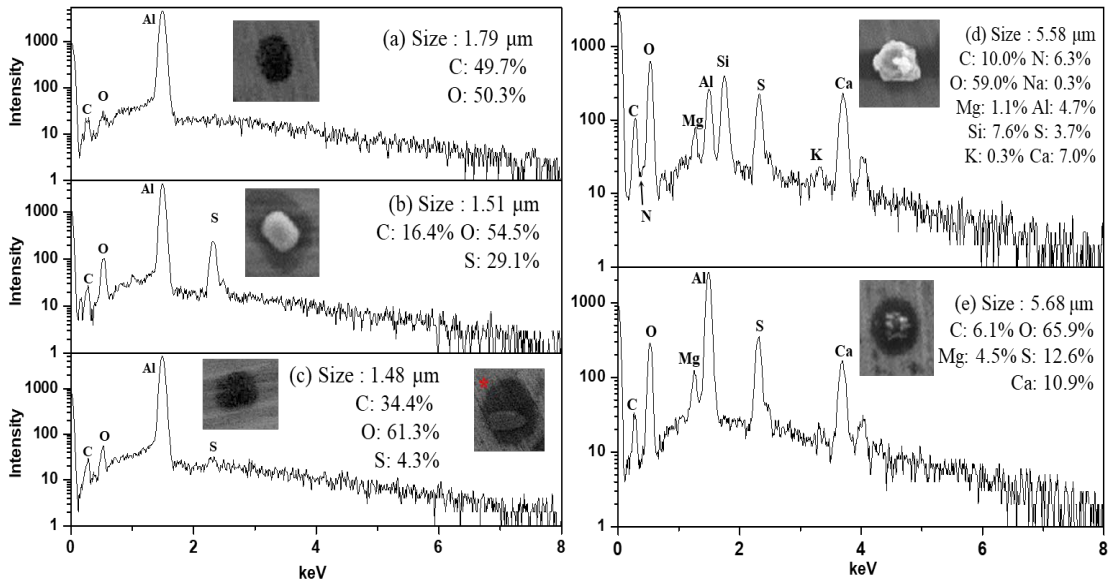

Figure 1. Morphology, X-ray spectra and elemental compositions of (a) SOA, (b) SOIA (high inorganic), (c) SOIA (high organic), (d) reacted aluminosilicate, and (e) reacted carbonate particles.

Genuine and reacted mineral dust particles are the most abundant particle types among the seven major ones in this study, accounting for 73.2% and 44.5% in the $PM_{2.5-10}$ and $PM_{1-2.5}$ fractions, respectively. These mineral dust particles are irregularly shaped and appear bright in SEI, mainly consisting of crustal elements such as Al, Si, Ca, Mg, K, and others. The observed chemical species of mineral dust particles include aluminosilicates (such as feldspar, muscovite, montmorillonite, illite, kaolinite, talc, pyrophyllite, etc.), quartz (SiO_2), carbonates (calcite ($CaCO_3$), dolomite ($CaMg(CO_3)_2$), and magnesite ($MgCO_3$)), TiO_2, and their reacted/aged ones. Genuine mineral dust particles, tending to be larger in size, are significantly more abundant in the $PM_{2.5-10}$ fraction than in the $PM_{1-2.5}$ fraction, whereas the proportion of reacted minerals is slightly higher in the $PM_{1-2.5}$ fraction (71.0%) compared to the $PM_{2.5-10}$ (66.2%) due to the larger specific surface area of $PM_{1-2.5}$ particles, making them more prone to chemical reactions in the air.

The reactivity of mineral dust particles varies depending on their chemical species and size, as shown in Table 1. In the $PM_{2.5-10}$ fractions, particles are highly associated with nitrate compared to sulfate (46.2% vs. 30.0%), while the abundance of sulfate is comparatively higher than nitrate for $PM_{1-2.5}$ particles (34.3% vs. 20.0%), indicating that sulfate formation occurs more frequently in smaller particles. The proportion of reacted particles is significantly higher in carbonate particles than in aluminosilicates (93.9% vs. 56.2%), indicating that carbonate mineral dust has a higher reactivity than aluminosilicates. Reacted aluminosilicate particles appear bright and irregular, being surrounded by water-soluble moieties (Fig. 1d), implying that the chemical reaction mostly occurred on the surface, while reacted carbonate species show dark lumpy, core-shell shapes (Fig. 1e), indicating that the reaction readily occurred from the

Table 1. Relative abundances of genuine and reacted mineral dust and SSA particles

Type		Genuine	Reacted (containing elements)			% of reacted particles		Total
			-N	-S	-both			
$PM_{2.5-10}$								
Mineral dust	Aluminosilicates	23.2%	17.9%	4.9%	5.8%	55.2%	66.3%	73.2%
	Carbonates	1.5%	8.5%	6.9%	4.5%	92.9%		
Sea spray aerosols		0%	4.5%	2.9%	5.1%	100.0%		12.5%
$PM_{1-2.5}$								
Mineral dust	Aluminosilicates	12.1%	5.0%	7.7%	3.4%	57.2%	70.9%	44.4%
	Carbonates	0.8%	3.6%	10.2%	1.6%	95.0%		
Sea spray aerosols		0%	4.4%	9.4%	2.0%	100.0%		15.8%

surface to the internal part. Further analysis reveals that the carbonate particles tend to react with sulfate, while aluminosilicates were more likely to interact with nitrate (Table 1). The different abundances of sulfate and nitrate in the reacted mineral particles not only depend on the particle species and size, but also on the source, transport pathway, and formation process (**Geng et al., 2011, 2014; Sullivan et al., 2007**). These findings suggest that (a) carbonate minerals are more sensitive to changes in atmospheric conditions than aluminosilicates, and (b) carbonate minerals react with sulfate before nitrate due to the prevailing neutralization by sulfate (**Takahashi et al., 2014; Matsuki et al., 2005; Seinfeld and Pandis., 2006; Sullivan et al., 2017**).

3.1.3 Sea-spray aerosols (SSAs)

Nascent SSAs are rich in characteristic elements such as Na, Mg, and Cl, as indicated by their X-ray spectra. They are released into the atmosphere from the sea surface through film drops and jet drops caused by bubble bursting (**Eom et al., 2016; Cochran et al., 2017**). Freshly emitted SSAs are a mixture of inorganic Na, Mg, and Cl and organic compounds such as fatty acids, amino acids, and liposaccharides, which are closely related to the biological activity of micro-organisms in the marine environment **(Eom et al., 2016; Cochran et al., 2017)**. Once released into the atmosphere, these nascent SSAs tend to react with various acidic species such as sulfuric, nitric, and organic acids to form reacted/aged SSAs. All SSAs for both $PM_{2.5-10}$ and $PM_{1-2.5}$ fractions were found to be in the reacted form (Table 1), despite their short transport distances (~50–100 km until they reach the sampling site from the Yellow Sea), suggesting that they are susceptible to atmospheric reactions **(Laskin et al., 2003; Gupta et al., 2015; Li et al., 2017; Chen et al., 2020).** As shown in Table 1, the reacted SSAs accounted for 12.4% and 15.7% in the $PM_{2.5-10}$ and $PM_{1-2.5}$ fractions, respectively, in which the nitrate-containing SSAs were more abundant than the sulfate-containing ones in the $PM_{2.5-10}$ fraction (9.6% vs. 8.4%), while those containing sulfates were more abundant in the $PM_{1-2.5}$ fraction (11.3 vs. 6.4%), indicating that sulfate formation occurs more in smaller SSA particles. The higher abundance of SSAs containing both nitrates and sulfates in the larger size fraction may be attributed to the availability of sufficient anions to accumulate acidic cations, which is associated with a decrease in acidity as particle size increases (**Angle et al., 2021).**

3.1.4 Combustion particles

The combustion particles include soot agglomerates, tar balls, fly ash, and char particles, accounting for 1.3% and 2.8% in the $PM_{2.5-10}$ and $PM_{1-2.5}$ fractions, respectively. Most

elemental carbon (EC) particles, such as soot agglomerates, tar balls, and char particles, have similar elemental compositions, but they can be differentiated based on their unique morphology (Fig. 2 and Table S1).

Soot agglomerates are remnants of incomplete combustion and are formed through the vaporization-condensation mechanism (**Bond et al., 2004; Chen et al., 2006**). Based on their morphology and elemental compositions, soot agglomerates can be classified into two types: fresh and aged. The fresh soot agglomerates appear bright and have a characteristic chain-like structure with fractal geometry, as shown in the right-side SEI of Fig. 2a. The complex geometry of the soot agglomerates provides an active area for the deposition of gaseous or particulate species. The morphology of aged soot agglomerates shown in Fig. 2a is more compact than that of the fresh ones. The aging of the soot agglomerates is attributed to several mechanisms such as oxidation, absorption or condensation of gaseous species, and coagulation with other particles. This aging process can cause the soot agglomerates to shrink and restructure into a more compact shape, as shown in Fig. 2a **(Bond et al, 2004; Zhang et al., 2008; Chen et al., 2006)**.

Tar ball particles are composed of organic oligomers and are a representative particle type from smoldering combustions such as biomass burning or biofuel combustion (**Adachi et al., 2019; Girotto et al., 2018; Pósfai et al., 2004**). The spherical shape of the tar ball particles (Fig. 2b) results from post-physical and chemical transformation of the organic matter. The formation of the tar balls can vary depending on factors such as oligomerization of organics, condensation, photochemical processes, water loss, and temperature changes, leading to different internal structures (**Tóth et al., 2018; Adachi et al., 2019**).

Char particles are incomplete combustion residues of liquid or solid carbonaceous fuel materials, appearing compact and irregular in shape on the SEI, as shown in Fig. 2c (**Chen et al., 2006**).

Fly ash particles, as shown in Fig. 2d, have a similar elemental composition to aluminosilicate mineral particles but with a distinct bright spherical shape on the SEI. These particles were rarely found in both size fractions, accounting for 0.08% and 0.42% in $PM_{2.5\text{-}10}$ and $PM_{1\text{-}2.5}$ fractions, respectively. The spherical morphology of fly ash particles is attributed to their formation mechanism, which involves rapid cooling after being released from high-temperature combustion at industrial plants **(Geng et al., 2011).**

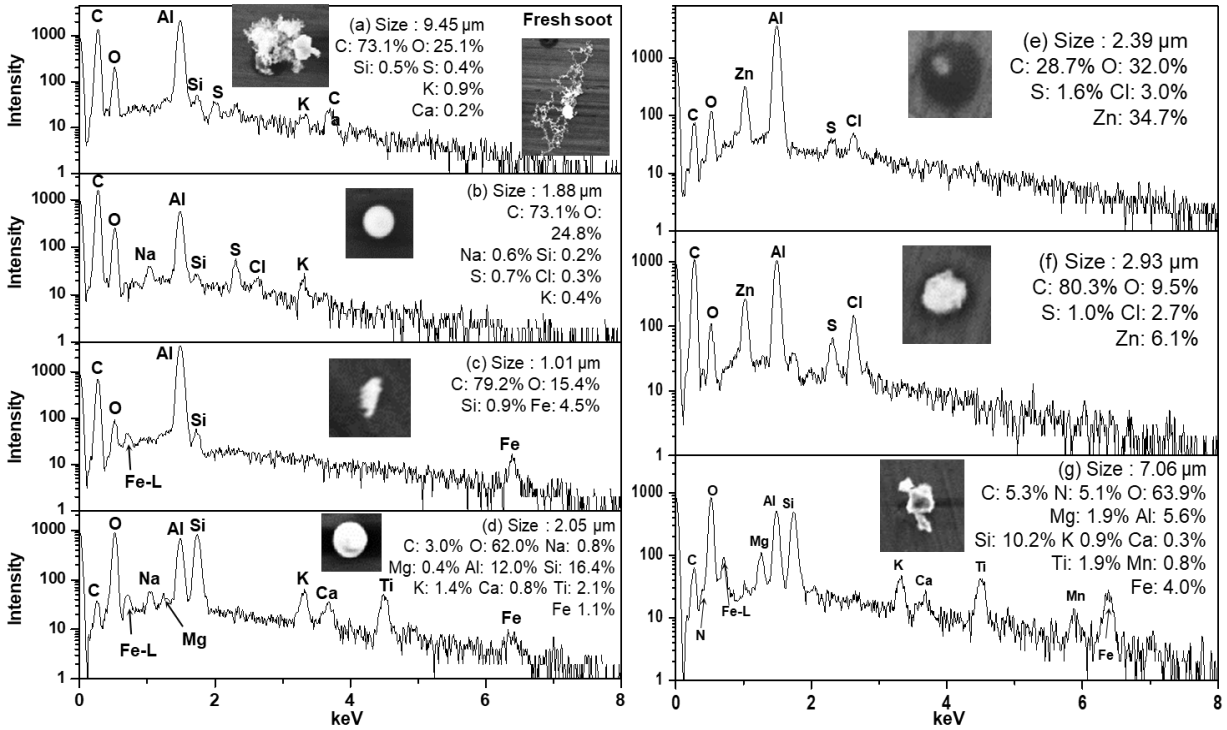

Figure 2. Morphology, X-ray spectra, and elemental compositions of (a) aged soot aggregates, (b) tar balls, (c) char, (d) fly ash, (e) and (f) Zn-HMs, and (g) Mn/Ti-HMs.

275

276 *3.1.5 Heavy metal-containing particles (HMs)*

277 Particles containing heavy metal elements (HMs), such as Zn, Pb, Cu, Mn, Ba, Zr, Sr,
278 Cd, As, Cr, V, Ni, Sn, and Co, are of particular concern due to their adverse impact on human
279 health. In this study, a significant number of HMs were observed, accounting for 2.7% and 4.4%
280 in the $PM_{2.5\text{-}10}$ and $PM_{1\text{-}2.5}$ fractions, respectively. Among the 14 types of HMs observed, Zn,
281 Pb, Ba, Cu, and Mn were frequently encountered (Fig. 3). HMs can be released from both
282 anthropogenic and natural sources, with thermal power plants, vehicle exhaust, battery
283 manufacture, and the metallurgical industry being some of the most common anthropogenic
284 sources (**Tian et al., 2015; Xu et al., 2004**). Tracing the sources of HMs during the KORUS-
285 AQ campaign can be done based on coexisting elements, morphologies, and relative
286 abundances.

287 As shown in Fig. 3, the most abundant type of HMs observed in this study were Zn-
288 containing particles (Zn-HMs), accounting for 32.3% and 58.0% of the total HMs in $PM_{2.5\text{-}10}$
289 and $PM_{1\text{-}2.5}$, respectively. Zn-HMs can be emitted from various anthropogenic sources such as
290 waste incineration, vehicle emissions, rubber tire wear, and coal combustion (**Hopke et al.,**
291 **1991; Chow et al., 2004; Hjortenkrans et al., 2007**). In the sampling site, which is an urban
292 area with heavy traffic, Zn-HMs may be attributed to vehicle emissions such as rubber tire and
293 brake pad wear. Two major identified types of Zn-HMs were C-Zn-Cl and C-Zn-Cl + (N or S)

(Fig. 2e and 2f), which made up 54.4% and 29.8% of the total Zn-HMs, respectively. A significant proportion (84.9%) of Zn-HMs were observed to contain Cl, likely due to incomplete atmospheric reactions of $ZnCl_2$. $ZnCl_2$ can easily undergo aqueous-phase chemical reactions in the atmosphere due to its hygroscopic nature. The presence of N or S on the X-ray spectra and dark droplet morphology on the SEI of the Zn-HMs indicate that the particles had undergone atmospheric reactions with NO_x/SO_x (**Moffet et al., 2008**). The temporal variations of Zn-HMs will be discussed in Section 3.2.

A total of 20 Pb-HMs were observed in this study, in the forms of mixtures with SSAs (8 particles), Pb-Cl-other heavy metals (6 particles), mineral dust (4 particles), and Pb-As (2 particles). They were likely emitted from vehicle exhaust and coal-fired power plants (**Lee et al., 2019b**). Among the 39 Mn-HMs observed, 24 particles were associated with mineral dust, coexisting mainly with Al, Si, Ca, and Mg; 6 particles with Fe; 2 particles with SSAs; 4 particles with Mg, Cl, and S; and 3 particles with F. They might originate from natural soil or anthropogenic sources such as ore-crushing plants, ferroalloy plants, and similar facilities (**Moreno et al., 2011**). The morphology and elemental composition of a Mn-HM are shown in Fig. 2g. Among the total 33 Cu-HMs, 17 particles were mixed with Fe, followed by the mineral dust form (10 particles), and minor forms such as Cu-C-S and Cu-C-N-O (6 particles). Major sources of atmospheric Cu include non-ferrous metal plants, mining, and smelting complexes (**Choi et al., 2013; Eichler et al., 2014**). Among the total of 30 Ba-HMs, 17 particles were

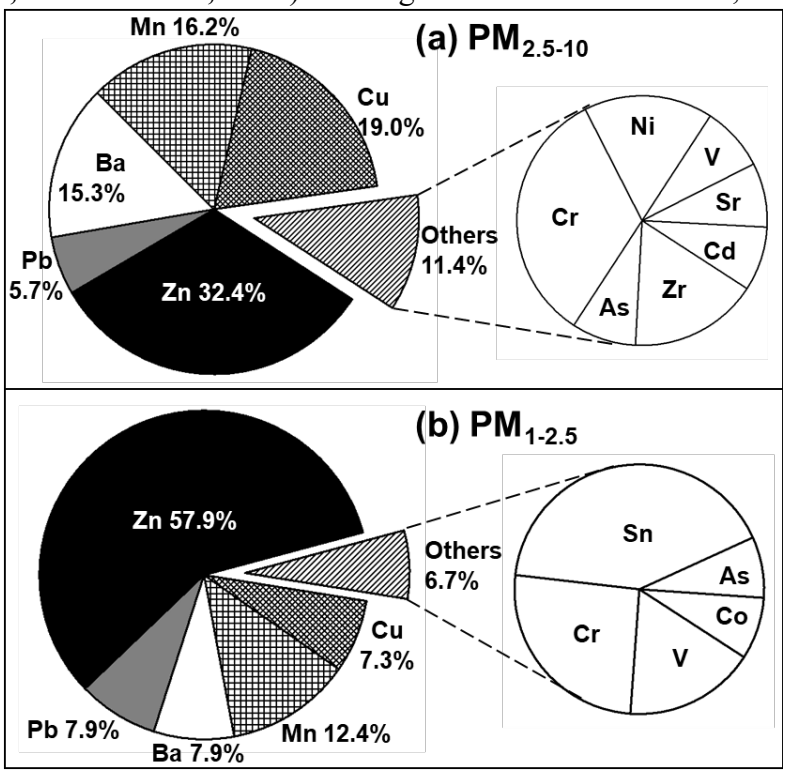

Figure 3. Heavy metals observed in HMs for (a) $PM_{2.5-10}$ and (b) $PM_{1-2.5}$ fractions.

mixed with Fe, followed by mineral dust (5 particles), $BaSO_4$ (3 particles), and other minor forms (5 particles). Ba-HMs could be released from natural sources in the form of barite ($BaSO_4$) and witherite ($BaCO_3$), and anthropogenic sources such as ore crushing plants, mining, refining, and manufacture of barium products (**Choudhury et al., 2009; Beddows et al., 2004**). The observation that Mn, Ba, and Cu-HMs appear abundantly as a mixture of Fe or mineral dust in this study suggests a possibility that their major source might be ferroalloy plants, mining, or ore crushing plants.

3.1.6 Fe-rich, biogenic, and HULIS particles

Fe-rich particles, which have an irregular shape and appear bright on the SEI, usually contain more than 20% Fe in elemental concentration. These particles account for 1.7% and 2.2% in the $PM_{2.5\text{-}10}$ and $PM_{1\text{-}2.5}$ fractions, respectively, and likely originate from steel production, metallurgical industries, and the abrasion of brake linings (**Geng et al., 2011**).

Biogenic particles, primarily originating from natural sources **(Martin et al., 2010)**, are relatively more abundant in the $PM_{2.5\text{-}10}$ fraction (2.83%) than the $PM_{1\text{-}2.5}$ fraction (0.81%). They can be identified by their unique morphologies and the presence of minor elements such as Na, Mg, N, K, P, S, and/or Cl **(Ro et al., 2002; Geng et al., 2011)**. In this study, most of the observed biogenic particles were attributed to trichomes, plant fragments, pollen, or spores, as their sizes were generally larger than 2 μm **(Matthias-Maser et al., 2000; Coz et al., 2010)**. Typical examples of biogenic particles are displayed in Fig. S2a-c, corresponding to fungal spores, micro-organism, and trichomes or leaf fragments, respectively.

The HULIS particles, consisting mainly of water-insoluble organic carbon (WISOC), are characterized by high C and O content and unique morphology. There are 17 out of 8004 particles, only accounting for 0.2%. They might be released from soil, wetland, and sewage-treatment plants.

3.2 Temporal chemical composition variations of individual aerosol particles during the KORUS-AQ campaign

Based on differences in relative abundances of individual particle types, ambient PM concentrations (Fig. S3), and backward air mass trajectories (Fig. S4), the sampling period (5/23–6/5) of the KORUS-AQ campaign was divided into five characteristic atmospheric situations as follows: (Period I, 5/23) - a SOA dominant period influenced by local emissions and air mass stagnation; (Period II, 5/25-5/28) - a SOIA-rich haze episode with the influence of long-range transported air-masses; (Period III, 5/29-5/31) - haze events with the combined

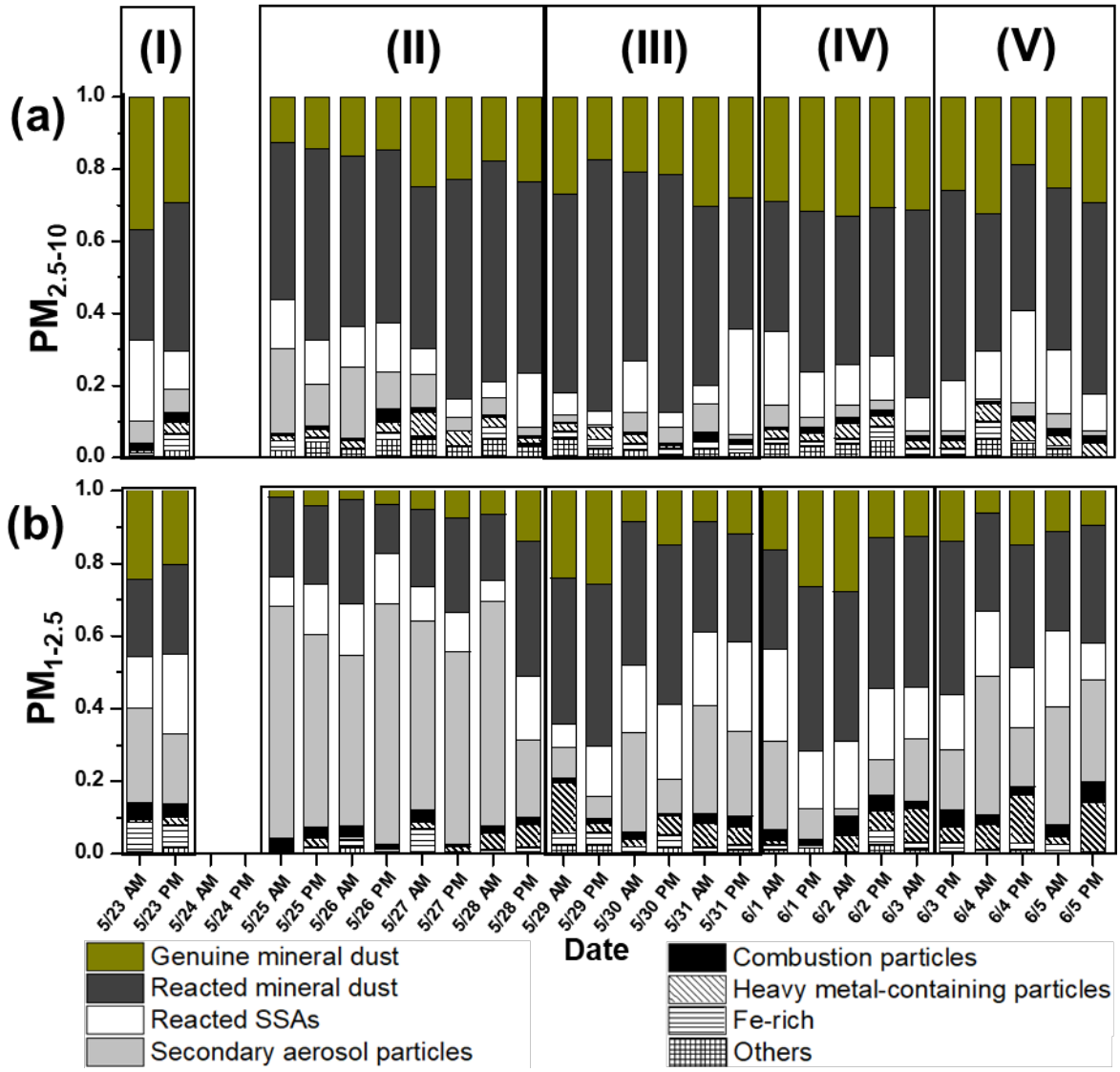

Figure 4. Relative abundances of various particle types in the (a) $PM_{2.5-10}$ and (b) $PM_{1-2.5}$ fractions.

influence of long-range transported air-masses and local emissions; (Period IV, 6/1-6/3) - a clean air period; and (Period V, 6/4-6/5) - a period dominantly influenced by local emissions. The relative abundances of individual particle types are shown in Fig. 4. There are significant differences over the sampling period, especially in the $PM_{1-2.5}$ fractions.

Period I (5/23)

On 5/23, the first day of the sampling period, individual aerosol particles showed clear distinctions in morphology and elemental compositions, particularly for secondary aerosol particles. As shown in Fig. 5a, most secondary aerosol particles in the $PM_{1\text{-}2.5}$ fraction, including SOA and SOIA, had dark droplet morphology, indicating that their major chemical species are organic carbon. Figure 6 highlights a significant increase in the ratio of SOA to secondary aerosol particles. The SOA/secondary aerosol particles ratio of the $PM_{1\text{-}2.5}$ fraction was notably higher (55.2%) in the 5/23 sample compared to the average for the overall samples during the campaign (22.0%), emphasizing the enhanced contribution of organic carbon to secondary aerosol particle formation. Figure 7 shows that the proportion of combustion particles increased by 1.8 and 1.6 times compared to the overall average in the $PM_{2.5\text{-}10}$ and $PM_{1\text{-}2.5}$ fractions, respectively. A slightly elevated PM concentration on 5/23 (Fig. S3) suggests mild air pollution on that day. Our findings align with other bulk studies that confirmed an increased proportion of organic carbon in PM_1 aerosols during 5/17-5/23 (**Kim et al., 2018a; Kim et al., 2018b**). Stagnant conditions under a persistent anticyclone prevented the transport

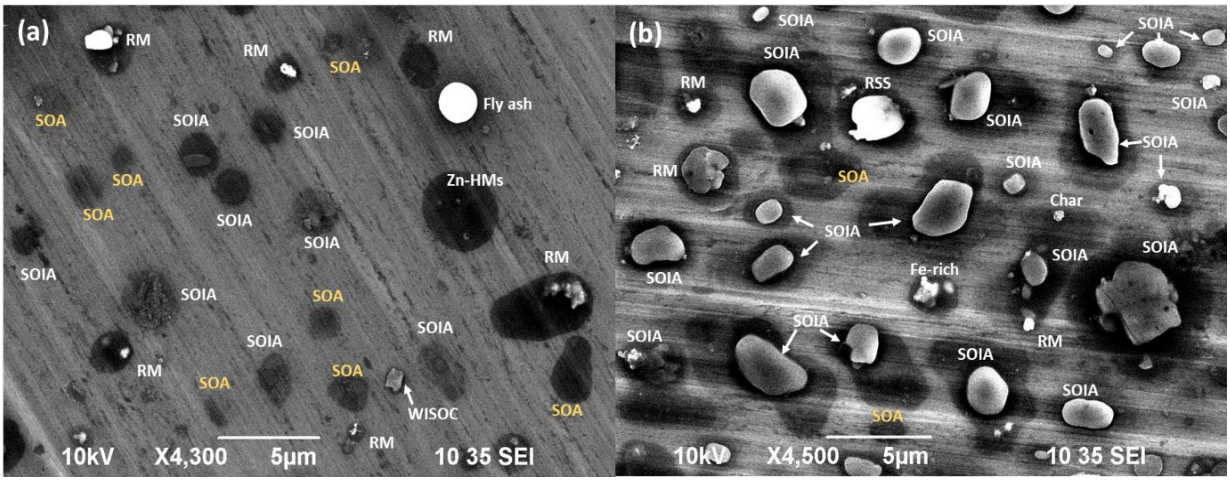

Figure 5. Typical secondary electron images of $PM_{1\text{-}2.5}$ aerosol particles collected on (a) 5/23 PM and (b) 5/25 AM. (RM : reacted mineral dust)

of pollutants from other regions, suggesting a dominant influence of local emissions during this period (**Kim et al., 2018b; Peterson et al., 2019; Heim et al., 2020**). The formation of SOA in South Korea, particularly in urban areas, was reported to be predominantly influenced by local emissions (**Nault et al., 2018**). Consequently, the rise in the proportion of organic carbon during Period I can be attributed to the augmented contribution of local emissions to the formation of secondary aerosol particles due to air mass stagnation (**Peterson et al., 2019; Kim et al., 2018a; Kim et al., 2018b; Crawford et al., 2021**). The enhanced level of combustion particles suggests the contribution of local emissions, while it also correlates with previous studies (Song et al., 2022; Peterson et al., 2019) that indicate additional influences

from Siberian wildfires between 5/20-5/23. Overall, the data from 5/23 indicate a clear influence of local emissions on aerosol particle composition and concentration.

Period II (5/25-5/28)

After the rainfall on 5/24, the morphology, elemental composition, and relative abundance of individual aerosol particles during 5/25-5/28 (Period II) differed significantly compared to those observed in Period I. In terms of particle morphology, Fig. 5b shows that SOIA particles on 5/25 exhibited a bright crystalline morphology, suggesting that these particles are primarily composed of inorganic components such as sulfate, nitrate, and ammonium, as described in Section 3.2.1. These bright crystalline SOIA particles mostly contain high sulfur contents, as shown in Fig. 1b, suggesting that their major composition is

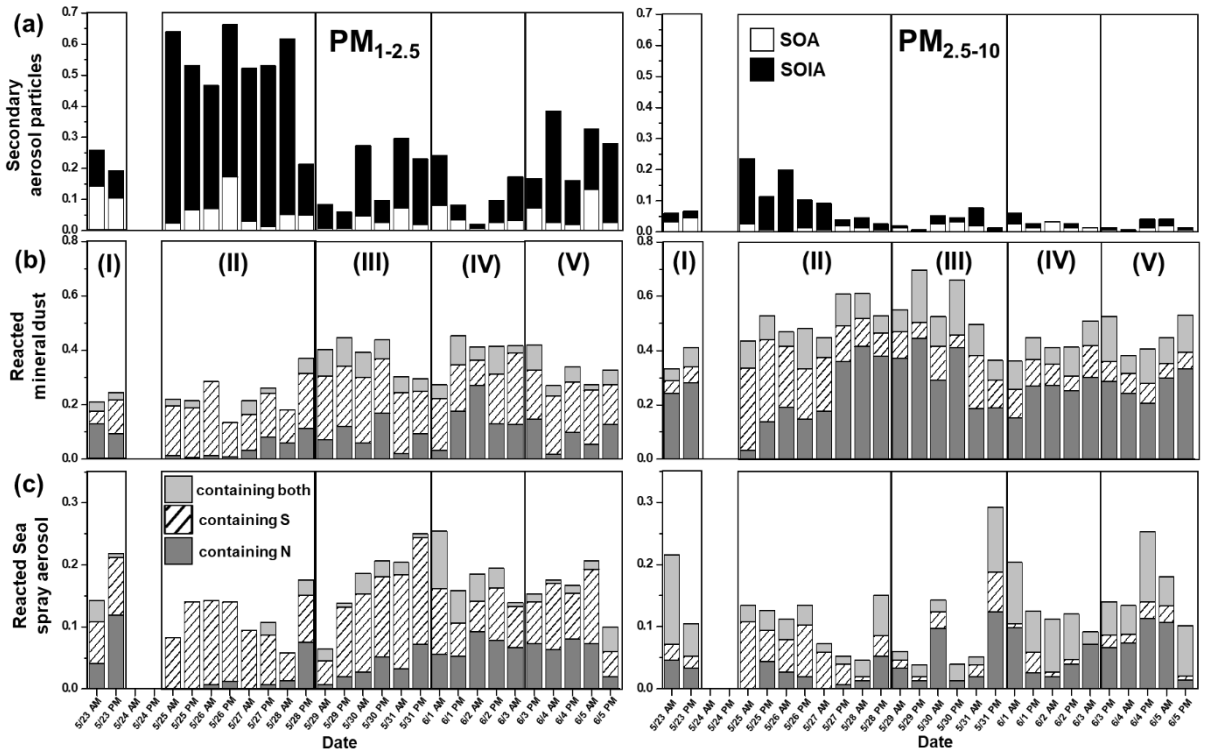

Figure 6. Relative abundances of (a) secondary aerosols, (b) reacted mineral dust, and (c) reacted SSA particles during the KORUS-AQ campaign.

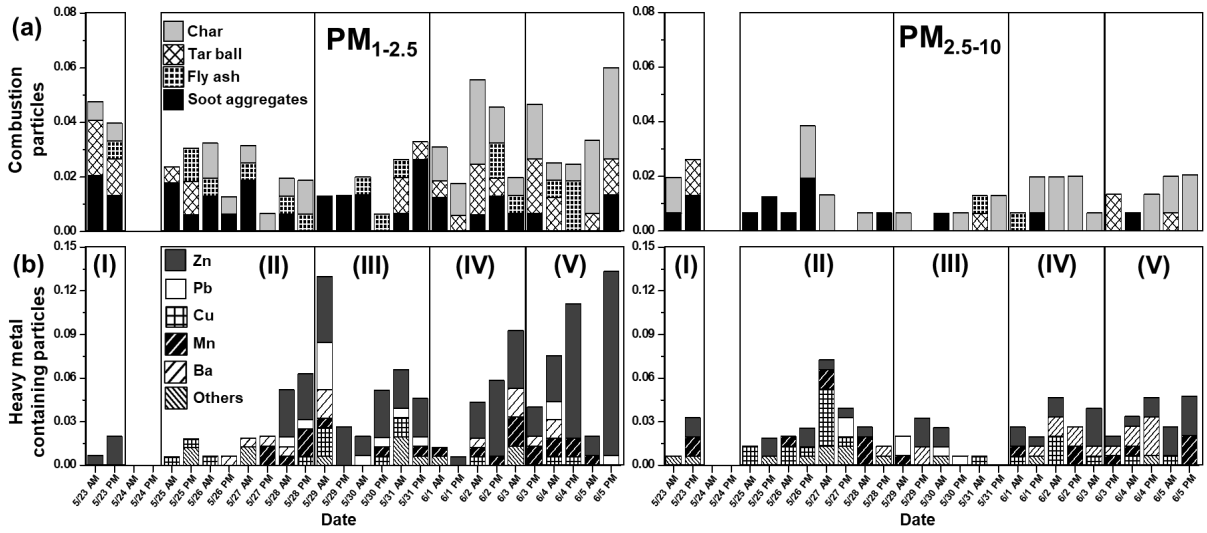

Figure 7. Relative abundances of (a) combustion particles and (b) heavy metal-containing particles during the KORUS-AQ campaign.

likely ammonium sulfate (AS) (**Wu et al., 2019**). Ammonium-rich conditions in East Asia facilitate the existence of secondary particles in AS or AN forms (**Kim et al., 2020; Kim et al., 2021**). The ratio of SOIA particles to total particles increased dramatically during Period II, as shown in Fig. 6. In the $PM_{1\text{-}2.5}$ fraction, the proportion of SOIA particles out of the total particles increased significantly to 61.5% on 5/25, compared to the overall average of 24%, and remained high at 46.3% during Period II. Additionally, the reacted/aged mineral dust and SSA particles containing sulfate were dominant during Period II both in the $PM_{1\text{-}2.5}$ and $PM_{2.5\text{-}10}$ fractions. The drastic increase in ambient PM concentration during this period (Figure S3) is indicative of an air pollution (haze) episode. In contrast to Period I, which is considered to be influenced mainly by local emissions due to air mass stagnation, the drastic increase in sulfate composition of secondary aerosols, reacted mineral dust, and reacted SSA particles during Period II seems to be driven by other external factors than local emissions. As shown in Fig. S4b, air mass transportation from northeastern China at low altitudes (250 m A.G.L) was observed during this haze episode, which contrasts with Period I. Mild southwesterly winds (<5 m/s) facilitate the transport of pollutants from China to the study region **(Peterson et al., 2019; Nault et al., 2018; Heim et al., 2020; Choi et al., 2019).** An elevated level of secondary inorganic constituents, including sulfate, nitrate, and ammonium, was also reported during this period (**Kim et al., 2018a; Kim et al., 2018b; Song et al., 2022**). The humid conditions (RH > 60%) sustained during this period provided a favorable environment for the formation of secondary particles (SIA and SOA) (**Peterson et al., 2019**). Also, sulfate-containing mineral dust and SSA particles were abundantly observed because the air masses were buffered rapidly with sulfate when they passed through urban and industrial areas during long-range

transportation (**Yu et al., 2020**). Overall, the data from Period II suggest a significant influence of long-range transported air masses from northeastern China on the composition and concentration of aerosol particles in the study region.

Period III (5/29-5/31)

The relative abundances of individual particles during 5/29-5/31 (Period III) differed from those of 5/25-5/28 (Period II), despite consistently high PM concentrations during the period (Fig. S3) and air mass flow from Northeastern China (Figs. S4c and S4d). During Period III, the proportion of SOIA particles decreased to 14.4% compared to 46.3% in Period II (Fig. 6). Concurrently, the proportions of reacted mineral dust and SSA particles increased with a noticeable increase in nitrate-containing ones (Fig. 6). The increase in nitrate-containing particles in the urban area suggests a strong influence of local emissions (**Yan et al., 2015**). Changes in the relative abundances of individual HM particles were also noticeable (Fig. 7). The proportion of Zn-HMs increased rapidly from 0.8% during Period II to 2.8% during Period III, suggesting an elevated influence of local emissions, given that the major sources of Zn-HMs are local emissions (section 3.1.5). The proportion of other HMs also somewhat increased to 2.8% compared to the overall average of 1.9%. The changes in the relative abundances of individual particles observed in this study are fairly different from other bulk studies in which air pollution episodes with consistently high inorganic contents were observed during 5/25-5/31 (**Kim et al., 2018a; Kim et al., 2018b**). Similar to Period II, weak westerly winds facilitated the transport of pollutants during Period III; however, the formation of secondary particles appears to be relatively reduced due to ~20% lower RH compared to Period II (**Peterson et al., 2019**). Additionally, as shown in Figs. S4b and S4c, during Period III, the travel distance and residence time within the Korean Peninsula were longer relative to Period II, suggesting an increased mixing of transported and local pollutants. Based on the decrease in the proportion of secondary aerosol particles formed mainly through gas-particle conversion and the increase in the reacted forms of the primary aerosol particles, including mineral dust and SSAs, it is plausible that aggregation or mixing between individual particles intensified during Period III. Overall, the changes in particle abundances during Period III indicate a complex interplay of local emissions and long-range transport. The decrease in secondary aerosol particles and the increase in reacted primary aerosol particles, along with the elevated proportions of Zn-HMs and other HMs, suggest intensified mixing of pollutants from various sources during this period.

Period IV (6/1-6/3)

After a series of air pollution episodes, ambient PM concentrations decreased drastically from 6/1 (Fig. S3). The relative abundance of individual particle types during 6/1-6/3 manifested distinct differences compared to Periods I-III. During Period IV, the proportion of secondary aerosol particles decreased to 12.9%, compared to an overall average of 29.2%, while the proportion of genuine mineral dust particles increased from an overall average of 12.9% to 18.3% (Fig. 4). An increase in nitrate-containing reacted mineral dust and SSA particles was observed in both size fractions (Fig. 6). Zn-HMs from local emissions were also frequently encountered during this period (Fig. 7). Moreover, an increase in tar balls and char particles was observed (Fig. 7). Increases in nitrate-containing particles, Zn-HMs, and combustion particles suggest an intensified influence of local emissions. Additionally, it was reported that a blocking pattern influenced by high atmospheric pressure was observed over East Asia during this period, which minimized the transportation of pollutants from other Asian mainland areas (**Heim et al., 2020; Peterson et al., 2019**). This blocking pattern could have contributed to the increased influence of local emissions and the observed rise in nitrate-containing particles, Zn-HMs, and combustion particles during Period IV. Overall, the data from Period IV suggest that local emissions played a dominant role in shaping the aerosol composition during this period, with limited influence from long-range transported air masses. The decrease in secondary aerosol particles and the increase in genuine mineral dust particles and locally emitted pollutants such as Zn-HMs and combustion particles further support this conclusion.

Period V (6/4-6/5)

Ambient PM concentrations slightly increased during Period V compared to Period IV (Fig. S3). There was a noticeable increase in Zn-HMs during this period, with the proportion of Zn-HM increasing from an average of 2.6% to 6.6%. This increase was particularly noticeable during the afternoon hours (Fig. 7) and might be related to heightened weekend traffic, as the sampling area is a park surrounded by thoroughfares (Fig. S1). In addition, the proportion of secondary aerosol particles increased drastically to 28.8% compared to 12.9% in Period IV, and the proportion of combustion particles somewhat increased to 3.6% compared to an average of 2.6%. Air mass trajectories shown in Fig. S4f suggest an intensified influence from inland Korea during Period V, resulting in the increased levels of particles from local emissions and secondary aerosol particles. When the air mass travels a short distance (~250 km/day), urban areas could be primarily influenced by local emissions (**Lee et al., 2019a**).

Continued blocking patterns from Period IV effectively exclude pollutant transport from outside areas, but occasionally lead to stagnant conditions (**Peterson et al., 2019**). Overall, the changes in particle abundances during Period V indicate an intensified influence of local emissions and secondary aerosol particles, likely due to weekend traffic and stagnant conditions. The increase in Zn-HMs and combustion particles further supports the impact of local anthropogenic emissions on air quality during this period. Efforts to manage and control local emission sources, including vehicle emissions, waste incineration, and fossil fuel combustions, could play a crucial role in improving air quality in the urban area.

4. Conclusions

Individual aerosol particles collected at Olympic Park, Seoul, Korea, during the KORUS-AQ campaign were analyzed using low-*Z* particle EPMA. A total of 8004 particles from 52 samples were examined to identify their chemical species, particle-particle variability, sources, and atmospheric fate. The major constituents in the $PM_{2.5-10}$ and $PM_{1-2.5}$ fractions were mineral dust, SSAs, and secondary aerosol particles. However, the relative abundance of individual particle types varied depending on changes in air mass flow and differences in emission sources. The reacted mineral dust and reacted SSA particles containing nitrate were abundant in the $PM_{2.5-10}$ fraction, whereas sulfate-containing ones were relatively higher in the $PM_{1-2.5}$ fraction. Of particular interest, heavy metals were found to account for a relatively high proportion of particles both in the $PM_{2.5-10}$ (2.65%) and $PM_{1-2.5}$ (4.42%) fractions, with Zn, Pb, Ba, Mn, and Cu being the major species. Zn and Pb are mainly released from sources such as waste incineration, vehicle exhaust, and coal-fired power plants, while Mn, Ba, and Cu are primarily released from mining and metal alloy industries.

The relative abundances of secondary aerosol particles varied significantly during the sampling period, reflecting changes in air mass stagnation and emission sources. During the haze episodes, sulfate-containing particles, including SOIA, mineral dust, and SSAs, were predominant, and the proportion of SOA particles increased as local influence intensified. During the clean period of 6/1-6/3, nitrate-containing particles were abundantly observed, indicating a high contribution of NO_x emissions from local sources. Zn-HMs from local sources such as vehicle emissions and waste incineration were noticeably observed during 6/4-6/5 when the air mass stagnated over the Korean peninsula.

The temporal variations in the abundance and physicochemical characteristics of individual aerosol particles provide valuable insights into the behavior and emission sources of atmospheric urban aerosols. The changes in the composition of organic and inorganic

components resulted in distinct morphological and crystalline structures of secondary aerosol particles, influencing properties such as hygroscopic behavior and radiative forcing. The relative abundance of HMs, particularly those containing Zn, effectively reveals the impact of local emissions such as vehicle emissions and waste incineration. The highly hygroscopic nature of the observed Zn-HMs suggests a potential threat to human health, as they are prone to adsorbing or reacting with other organic and inorganic components in the atmosphere. The observed changes in the abundance of particles from typical combustion events and secondary aerosol particles emphasize the need to manage local emission sources to maintain air quality. The complexity of aerosol particle behavior highlights the importance of a comprehensive understanding of the interplay between local emissions, long-range transport, and meteorological conditions to develop effective air pollution mitigation strategies.

Code and data availability

The data set is available upon request from Chul-Un Ro (curo@inha.ac.kr).

Author contributions

Chul-Un Ro (RCU) and **Geng Hong (GH)** designed and supervised the entire experimental program, provided guidance on the quantitative analysis of individual particles, and reviewed the manuscript. **Hanjin Yoo (HJY)** conducted the single-particle analysis, analyzed the data, and wrote the manuscript. **Li Wu (LW)** reviewed the manuscript and provided feedback on the manuscript. All authors read and approved the final manuscript.

Competing interests

The authors declare that they have no conflict of interest.

Financial Support

This study was supported by the National Research Foundation of Korea (NRF) grant funded by the Korean government (MSIT) (No. 2021R1A4A1032579 and No. 2021R1A2C2004240) and by the National Institute of Environmental Research (NIER) funded by the Ministry of Environment (MOE) of Korea (NIER-2021-03-03-007). The authors thank for a fund from the China State High-end Foreign Expert Recruitment Project (G2022004013L).

Supporting Information

Table S1 and Figures S1-S4

References

Adachi, K., & Buseck, P. R.: Changes of ns-soot mixing states and shapes in an urban area during CalNex. J. Geophys. Res.-Atmos., 118(9), 3723-3730. https://doi.org/10.1002/jgrd.50321, 2013.

Adachi, K., Sedlacek, A. J., Kleinman, L., Springston, S. R., Wang, J., Chand, D., Hunne, J. M., Shilling, J. E., Onasch, T. B., Kinase, T., Sakata, K., Takahashi, Y., and Buseck, P. R.: Spherical tarball particles from through rapid chemical and physical changes of organic matter in biomass-burning smoke, Proc. Natl. Acad. Sci. U.S.A, 116, 19336-19341, www.pnas.org/cgi/doi/10.1073/pnas.1900129116, 2019.

Andreae, M. O., and Rosenfeld, D.: Aerosol-cloud-precipitation interactions. Part 1. The nature and sources of cloud-active aerosols, Earth Sci. Rev., 89, 13-41, doi:10.1016/j.earscirev.2008.03.001, 2008.

Angle, K. J., Crocker, D. R., Simpson, R. M. C., Mayer, K. J., Garofalo, L. A., Moore, A. N., Garcia, S. L. M., Or, V. W., Srinivasan, S., Farhan, M., Sauer, J. S., Lee, C., Pothier, M. A., Farmer, D. K., Martz, T. R., Bertram, T. H., Cappa, C. D., Prather, K. A., and Grassian, V. H.: Acidity across the interface from the ocean surface to sea spray aerosol, Proc. Natl. Acad. Sci. U.S.A, 118(2), e2018397118, https://doi.org/10.1073/pnas.2018397118, 2021.

Beddows, D. C. S., Donova, R. J., Harrison, R. M., Heal, M. R., Kinnersley, R. P., King, M. D., Nicholson, D. H., and Thompson, K. C.: Correlations in the chemical composition of rural background atmospheric aerosol in UK determined in real time using time-of-flight mass spectrometry, J. Environ. Monit., 6, 124-133, https://doi.org/10.1039/B311209H, 2004.

Bond, T. C., Streets, D. G., Yarber, K. F., Nelsom, S. M., Woo, J.-H., and Klimont, Z.: A technology-based global inventory of black and organic carbon emissions from combustion, J. Geophys. Res., 109, D14203, doi:10.1029/2003JD003697, 2004.

Chen, L., Peng, C., Gu, W., Fu, H., Jian, X., Zhang, H., Zhang, G., Zhu, J., Wang, X., and Tang, M.: On mineral dust aerosol hygroscopicity, Atmos. Chem. Phys., 20, 13611–13626, https://doi.org/10.5194/acp-20-13611-2020, 2020.

Chen, S., Huang, J., Kang, L., Wang, H., Ma, X., He, Y., Yuan, T., Yang, B., Huang, Z., and Zhang, G.: Emission, transport, and radiative effects of mineral dust from the Taklimakan and Gobi deserts: Comparison of measurements and model results, Atmos. Chem. Phys., 17, 2401–2421, https://doi.org/10.5194/acp-17-2401-2017, 2017.

Chen. Y., Shah, N., Huggins, F. E., and Huffman, G. P.: Microanalysis of ambient particles form Lexington, KY, by electron microscopy, Atmos. Environ., 40, 651-663, doi:10.1016/j.atmosenv.2005.09.036, 2006.

Cho, C., Schwarz, J. P., Perring, A. E., Lamb, K. D., Kondo, Y., Park, J. U., Park, D. H., Shim, K., Park, J. S., Park, R. J., Lee, M., Song, C. K., and Kim, S. W.: Light-absorption enhancement of black carbon in the Asian outflow inferred from airborne SP2 and in-situ measurements during KORUS-AQ, Sci. Tot. Environ., 773, https://doi.org/10.1016/j.scitotenv.2021.145531, 2021.

Choi, J. kyu, Heo, J. B., Ban, S. J., Yi, S. M., and Zoh, K. D.: Source apportionment of PM2.5 at the coastal area in Korea, Sci. Tot. Environ., 447, 370–380, https://doi.org/10.1016/j.scitotenv.2012.12.047, 2013.

Choi, J., Park, R. J., Lee, H.-M., Lee, S., Jo, D. S., Jeong, J. I., Henze, D. K., Woo, J.-H., Ban, S.-J., and Lee, M.-D.: Impacts of local vs. trans-boundary emissions from different sectors on PM2. 5 exposure in South Korea during the KORUS-AQ campaign, Atmos. Environ., 203, 196-205, 10.1016/j.atmosenv.2019.02.008, 2019.

Choi, Y., Ghim, Y. S., Rozenhaimer, M. S., Redemann, J., LeBlanc, S. E., Flynn, C. J., Johnson, R. J., Lee, Y., Lee, T., Park, T., Schwarz, J. P., Lamb, K. D., and Perring, A. E.: Temporal and spatial variations of aerosol optical properties over the Korean Peninsula during KORUS-AQ, Atmos. Environ., 254, 118301, https://doi.org/10.1016/j.atmosenv.2021.118301, 2021.

Choudhury, H., Carey, R.: Barium and barium compounds, Concise Int. Chem. Assessment Doc. 33. Int. Progr. Chem. Safety, World Health Organ., Geneva, 2009.

Chow, J. C., Watson, J. G., Kuhns, H., Etyemezian, V., Lowenthal, D. H., Crow, D., Kohl, S. D., Engelbrecht, J. P., and Green, M. C.: Source profiles for industrial, mobile, and area sources in the Big Bend Regional Aerosol Visibility and Observational study, Chemosphere, 54, 185-208, 10.1016/j.chemosphere.2003.07.004, 2004.

Chowdhury, P. H., He, Q., Male, T. L., Brune, W. H., Rudich, Y., and Pardo, M.: Exposure of lung epithelial clls to photochemically aged secondary organic aerosol shows increased toxic effects, Environ. Sci. Technol. Lett., 5, 424-430, doi:10.1021/acs.estlett.8b00256, 2018.

Cochran, R. E., Laskina, O., Trueblood, J. V., Estillore, A. D., Morris, H. S., Jayarathne, T., Sultana, C. M., Lee, C., Lin, P., Laskin, J., Laskin, A., Dowling, J. A., Qin, Z., Cappa, C. D., Bertram, T. H., Tivanski, A. V., Stone, E. A., Prather, K. A., and Grassian, V. H.: Molecular diversity of sea spray aerosol particles: impact of ocean biology on particle composition and hygroscopicity, Chem, 2(5), 655-667, https://doi.org/10.1016/j.chempr.2017.03.007, 2017.

Coz, E., Artíñano, B., Clark, L. M., Hernandez, M., Robinson, A. L., Casuccio, G. S., Lersch, T. L., and Pandis, S. N.: Characterization of fine primary biogenic organic aerosol in an urban area in the northeastern United States, Atmos. Environ., 44(32), 3952-3962, https://doi.org/10.1016/j.atmosenv.2010.07.007, 2010.

Crawford, J. H., Ahn, J.-Y., Al-Saadi, J., Change, L., Emmons, L. K., Kim, J., Lee, G., Park, J.-H., Park, R. J., Woo, J. H., Song, C.-K., Hong, J.-H., Hong, Y.-D., Lefer, B. L., Lee, M., Lee, T., Kim, S., Min, K.-E., Yum, S.-Y., Shin, H. J., Kim, Y.-W., Choi, J.-S., Park, J.-S., Szykman, J. J., Long, R. W., Jordan, C. E., Simpson, I. J., Fried, A., Dibb, J. E., Cho, S. Y., Kim, Y. P.: The Korea–United States Air Quality (KORUS-AQ) field study, Elementa. 9., 00163, https://doi.org/10.1525/elementa.2020.00163, 2021.

Eichler, A., Tobler, L., Eyrikh, S., Malygina, N., Papina, T., and Margit, S.: Ice-core based assessment of historical anthropogenic heavy metal (Cd, Cu, Sb, Zn) emissions in the Soviet Union, Enivron. Sci. Technol., 48, 2635-2642, dx.doi.org/10.1021/es404861n, 2014.

Eom, H. J., Gupta, D., Cho, H. R., Hwang, H. J., Hur, S. D., Gim, Y., and Ro, C. U.: Single-particle investigation of summertime and wintertime Antarctic sea spray aerosols using low-Z particle EPMA, Raman microspectrometry, and ATR-FTIR imaging techniques, Atmos. Chem. Phys., 16, 13823–13836, https://doi.org/10.5194/acp-16-13823-2016, 2016.

Geng, H., Jung, H.-J., Park, Y., Hwang, H., Kim, H., Kim, Y. J., Sunwoo, Y., and Ro, C.-U.: Morphological and chemical composition characteristics of summertime atmospheric particles collected at Tokchok Island, Korea, Atmos. Environ., 43, 3364-3373, 10.1016/j.atmosenv.2009.03.034, 2009.

Geng, H., Ryu, J., Maskey, S., Jung, H.-J., and Ro, C.-U.: Characterization of individual aerosol particles collected during a haze episode in Incheon, Korea using the quantitative ED-EPMA technique, Atmos. Chem. Phys., 10, 26641-26676, 10.5194/acp-11-1327-2011, 2011.

Geng, H., Hwang, H., Liu, X., Dong, S., and Ro, C.-U.: Investigation of aged aerosols in size-resolved Asian dust storm particles transported from Beijing, China, to Incheon, Korea,

using low-Z particle EPMA, Atmos. Chem. Phys., 14, 3307, 10.5194/acp-14-3307-2014, 2014.
Girotto, G., China, S., Bhandari, J., Gorkowski, K., Scarnato, B. v., Capek, T., Marinoni, A., Veghte, D. P., Kulkarni, G., Aiken, A. C., Dubey, M., and Mazzoleni, C.: Fractal-like Tar Ball Aggregates from Wildfire Smoke, Environ. Sci. Technol. Lett., 5, 360–365, https://doi.org/10.1021/acs.estlett.8b00229, 2018.
Gupta, D., Eom, H.-J., Cho, H.-R., and Ro, C.-U.: Hygroscopic behavior of NaCl–MgCl2 mixture particles as nascent sea-spray aerosol surrogates and observation of efflorescence during humidification, Atmos. Chem. Phys., 15, 11273-11290, https://doi.org/10.5194/acp-15-11273-2015, 2015.
Hallquist, M., Wenger, J. C., Baltensperger, U., Rudich, Y., Simpson, D., Claeys, M., Dommen, J., Donahue, N. M., George, C., Goldstein, A. H., Hamilton, J. F., Herrmann, H., Hoffmann, T., Iinuma, Y., Jang, M., Jenkin, M. E., Jimenez, J. L., Kiendler-Scharr, A., Maenhaut, W., McFiggans, G., Mentel, Th. F., Monod, A., Prévôt, A. S. H., Seinfeld, J. H., Surratt, J. D., Szmigielski, R., and Wildt, J.: The formation, properties and impact of secondary organic aerosol: current and emerging issues, Atmos. Chem. Phys., 9, 5155–5236, https://doi.org/10.5194/acp-9-5155-2009, 2009.
Heim, E. W., Dibb, J., Scheuer, E., Jost, P. C., Nault, B. A., Jimenez, J. L., Peterson, D., Knote, C., Fenn, M., Hair, J., Beyersdorf, A. J., Corr, C., and Anderson, B. E.: Asian dust observed during KORUS-AQ facilitates the uptake and incorporation of soluble pollutants during transport to South Korea, Atmos. Environ., 224, https://doi.org/10.1016/j.atmosenv.2020.117305, 2020.
Hjortenkrans, D. S., Bergbäck, B. G., and Häggerud, A. V.: Metal emissions from brake linings and tires: case studies of Stockholm, Sweden 1995/1998 and 2005, Environ. Sci. Technol., 41, 5224-5230, 10.1021/es070198o, 2007.
Hopke, P. K.: An introduction to receptor modeling, Chemometrics and Intelligent Laboratory Systems, 10, 21-43, 10.1016/0169-7439(91)80032-L, 1991.
IPCC, 2021: Climate Change 2021: The Physical Science Basis. Contribution of Working Group I to the Sixth Assessment Report of the Intergovernmental Panel on Climate Change [Masson-Delmotte, V., P. Zhai, A. Pirani, S.L. Connors, C. Péan, S. Berger, N. Caud, Y. Chen, L. Goldfarb, M.I. Gomis, M. Huang, K. Leitzell, E. Lonnoy, J.B.R. Matthews, T.K. Maycock, T. Waterfield, O. Yelekçi, R. Yu, and B. Zhou (eds.)]. Cambridge University Press. In Press.
Kim, E., Kim, B.-U., Kim, H. C., and Kim, S.: Direct cross impacts of upwind emission control on downwind PM2.5 under various NH3 conditions in Northeast Asia, Environ. Pollut., 268, 115794, https://doi.org/10.1016/j.envpol.2020.115794, 2021.
Kim, N., Park, M., Yum, S. S., Park, J. S., Shin, H. J., and Ahn, J. Y.: Impact of urban aerosol properties on cloud condensation nuclei (CCN) activity during the KORUS-AQ field campaign, Atmos. Environ., 185, 221-236, 0.1016/j.atmosenv.2018.05.019, 2018a.
Kim, N., Yum, S. S., Park, M., Park, J. S., Shin, H. J., and Ahn, J. Y.: Hygroscopicity of urban aerosols and its link to size-resolved chemical composition during spring and summer in Seoul, Korea, Atmos. Chem. Phys., 20, 11245–11262, https://doi.org/10.5194/acp-20-11245-2020, 2020.
Kim, H., Zhang, Q., and Heo, J.: Influence of intense secondary aerosol formation and long-range transport on aerosol chemistry and properties in the Seoul Metropolitan Area during spring time: results from KORUS-AQ, Atmos. Chem. Phys., 18, 7149-7168, https://doi.org/10.5194/acp-18-7149-2018, 2018b.
Kumar, N., Park, R. J., Jeong, J. I., Woo, J.-H., Kim, Y., Johnson, J., Yarwood, G., Kang, S., Chun, S., and Knipping, E.: Contributions of international sources to PM2.5 in South

693 Korea, Atmos. Environ., 261, 118542, https://doi.org/10.1016/j.atmosenv.2021.118542,
694 2021.
695 Laskin, A., Gaspar, D. J., Wang, W., Hunt, S. W., Cowin, J. P., Colson, S. D., and Finlayson-
696 Pitts, B. J.: Reactions at interfaces as a source of sulfate formation in sea-salt particles,
697 Science, 301(5631), 340-344, DOI:10.1126/science.1085374, 2003.
698 Lee, S., Kim, J., Choi, M., Hong, J., Lim, H., Eck, T. F., Holben, B. N., Ahn, J. Y., Kim, J.,
699 and Koo, J. H.: Analysis of long-range transboundary transport (LRTT) effect on
700 Korean aerosol pollution during the KORUS-AQ campaign, Atmos. Environ., 204, 53–
701 67, https://doi.org/10.1016/j.atmosenv.2019.02.020, 2019a.
702 Lee, S., Shin, D., Han, C., Choi, K.-S., Hur, S. D., Lee, J., Byun, D.-S., Kim, Y.-T., and Hong,
703 S.: Characteristic concentrations and isotopic composition of airborne lead at urban,
704 rural and remote sites in western Korea, Environ. Pollut., 254, 113050,
705 https://doi.org/10.1016/j.envpol.2019.113050, 2019b.
706 Li, W., Teng, X., Chen, X., Liu, L., Xu, L., Zhang, J., Wang, Y., Zhang, Y., Shi, Z.: Organic
707 Coating Reduces Hygroscopic Growth of Phase-Separated Aerosol Particles. Environ.
708 Sci. Technol., 55(24), 16339-16346, https://doi.org/10.1021/acs.est.1c05901, 2021.
709 Li, X., Gupta, D., Lee, J., Park, G., and Ro, C.-U.: Real-time investigations of chemical
710 compositions and hygroscopic properties of aerosols generaged from NaCl and Malonic
711 acid solutions using in situ Raman microscpectrometry, Environ. Sci. Tehcnol., 51(1),
712 263-270, https://doi.org/10.1021/acs.est.6b04356, 2017.
713 Martin, S. T., Andreae, M. O., Artaxo, P., Baumgardner, D., Chen, Q., Goldstein, A. H.,
714 Guenther, A., Heald, C. L., Mayol-Bracero, O. L., McMurry, P. H., Pauliquevis, T.,
715 Pöschl, U., Prather, K. A., Roberts, G. C., Saleska, S. R., Silva Dias, M. A., Spracklen,
716 D. V., Swietlicki, E., and Trebs, I.: Sources and properties of Amazonian aerosol
717 particles, Rev. Geophys., 48, RG2002, 10.1029/2008rg000280, 2010.
718 Matsuki, A., Iwasaka, U., Shi, G., Zhang, D., Trochkine, D., Yamada, M., Kim, Y.-S., Chen,
719 B., Nagatani, T., Miyazawa, T., Nagatani, M., and Nakata, H.: Morphological and
720 chemical modification of mineral dust: Observational insight into the heterogeneous
721 uptake of acidic gases, Geophys. Res. Lett., 32, 1-4, doi:10.1029/2005GL024176, 2005.
722 Matthias-Maser, S., Obolkin, V., Khodzer, T., and Jaenicke, R.: Seasonal variation of primary
723 biological aerosol particles in the remote continental region of Lake Baikal/Siberia,
724 Atmos. Environ., 34, 3805-3811, doi.org/10.1016/S1352-2310(00)00139-4, 2000.
725 Moffet, R. C., Desyaterik, Y., Hopkins, R. J., Tivanski, A. V., Gilles, M. K., Wang, Y.,
726 Shutthanandan, V., Molina, L. T., Abraham, R. G., and Johnson, K. S.: Characterization
727 of aerosols containing Zn, Pb, and Cl from an industrial region of Mexico City, Environ.
728 Sci. Technol., 42, 7091-7097, 10.1021/es7030483, 2008.
729 Moreno, T., Pandolfi, M., Querol, X., Lavín, J., Alastuey, A., Viana, M., and Gibbons, W.:
730 Mangaese in the urban atmosphere: identifying anamalous concentrations and sources,
731 Environ. Sci. Pollut. Res, 18, 173-183, DOI 10.1007/s11356-010-0353-8, 2011.
732 Nault, B. A., Campuzano-Jost, P., Day, D. A., Schroder, J. C., Anderson, B., Beyersdorf, A. J.,
733 Blake, D. R., Brune, W. H., Choi, Y., Corr, C. A., de Gouw, J. A., Dibb, J., Digangi, J.
734 P., Diskin, G. S., Fried, A., Gregory Huey, L., Kim, M. J., Knote, C. J., Lamb, K. D.,
735 Lee, T., Park, T., Pusede, S. E., Scheuer, E., Thornhill, K. L., Woo, J. H., and Jimenez,
736 J. L.: Secondary organic aerosol production from local emissions dominates the organic
737 aerosol budget over Seoul, South Korea, during KORUS-AQ, Atmos. Chem. Phys., 18,
738 17769–17800, https://doi.org/10.5194/acp-18-17769-2018, 2018.
739 Park, M., Yum, S. S., Kim, N., Anderson, B. E., Beyersdorf, A., Thornhill, K. L.: On the
740 submicron aerosol distributions and CCN activity in and around the Korean Peninsula
741 measured onboard the NASA DC-8 research aircraft during the KORUS-AQ field

campaign, Atmos. Res., 243, 105004, https://doi.org/10.1016/j.atmosres.2020.105004, 2020.
Park, S., Yu, G. H., and Lee, S.: Optical absorption characteristics of brown carbon aerosols during the KORUS-AQ campaign at an urban site, Atmos. Res., 203, 16–27, https://doi.org/10.1016/j.atmosres.2017.12.002, 2018.
Peterson, D. A., Hyer, E. J., Han, S.-O., Crawford, J. H., Park, R. J., Holz, R., Kuehn, R. E., Eloranta, E., Knot, C., Jordan, C. E., and Lefer, B. L.: Meteorology influencing springtime air quality, pollution transport, and visibility in Korea, Elementa. 9., 7, 57, https://doi.org/10.1525/elementa.395, 2019.
Pochanart, P., Wild, O., and Akimoto, H. (2004). Air pollution import to and export from East Asia. In: Stohl, A. (eds) Air Pollution. The Handbook of Environmental Chemistry, vol 4G. Springer, Berlin, Heidelberg. https://doi.org/10.1007/b94525
Pósfai, M., Gelencsér, A., Simonics, R., Arató, K., Li, J., Hobbs, P. v., and Buseck, P. R.: Atmospheric tar balls: Particles from biomass and biofuel burning, J. Geophys. Res. Atmos., 109, https://doi.org/10.1029/2003jd004169, 2004.
Ramachandran, S., Rupakheti, M., and Lawrence, M. G.: Aerosol-induced atmospheric heating rate decreases over South and East Asia as a result of changing content and composition. Sci. Rep., 10, 20091, doi.org/10.1038/s41598-020-76936-z, 2020.
Ro, C.-U., Oh, K.-Y., Kim, H., Kim, H., Kim, H., Kim, Y. P., Lee, C. B., Kim, K.-H., Kang, C. H., and Osán, J.: Single-particle analysis of aerosols at Cheju Island, Korea, using low-Z electron probe X-ray microanalysis: A direct proof of nitrate formation from sea salts, Environ. Sci. Tchnol., 35, 4487-4494, 10.1021/es0155231, 2001.
Ro, C.-U., Kim, H., Oh, K.-Y., Yea, S. K., Lee, C. B., Jang, M., and Van Grieken, R.: Single-particle characterization of urban aerosol particles collected in three Korean cities using low-Z electron probe X-ray microanalysis, Environ. Sci. Technol., 36, 4770-4776, 10.1021/es025697y, 2002.
Rolph, G., Stein, A., and Stunder, B.: Real-time environmental applications and display sYstem: ready. Environ. Model. Softw. 95, 210–228. doi: 10.1016/j.envsoft.2017.06.025, 2017.
Seinfeild, J. H., and Pandis, S. N.: Atmospheric chemistry and physics: from air pollution to climate chagnes. 2nd edition, John Wileyu & Sons, New york, 2006.
Sobanska, S., Hwang, H., Choël, M., Jung, H. J., Eom, H. J., Kim, H., Barbillat, J., and Ro, C. U.: Investigation of the chemical mixing state of individual asian dust particles by the combined use of electron probe X-ray microanalysis and raman microspectrometry, Anal. Chem., 84, 3145–3154, https://doi.org/10.1021/ac2029584, 2012.
Song, M., Park, J., Lim, Y., Oh, S.-H., Lee, J. Y., Lee, K.-H., Ro, C.-U., and Bae, M.-S.: Long-range transport impacts from biomass burning and secondary pollutant sources based on receptor models during KORUS-AQ campaign, Atmos. Environ., 276, 119060, https://doi.org/10.1016/j.atmosenv.2022.119060, 2022.
Stein, A., Draxler, R. R., Rolph, G. D., Stunder, B. J., Cohen, M., and Ngan, F.: NOAA's HYSPLIT atmospheric transport and dispersion modeling system, Bull. Am. Meteorol. Soc. 96, 2059–2077. doi: 10.1175/BAMS-D-14-00110.1, 2015.
Sullivan, R. C., Guazzotti, S. A., Sodeman, D. A., and Prather, K. A.: Direct observations of the atmospheric processing of Asian mineral dust, Atmos. Chem. Phys., 7, 1213–1236, https://doi.org/10.5194/acp-7-1213-2007, 2007.
Takahashi, Y., Higashi, N., Furukawa, T., Miyoshi, T., Fujiwara, M., and Uematsu, M.: A study of the chemical processes in aerosols and their impacts on the environment using X-ray absorption fine structure spectroscopy, W-PASS., 43-50, doi:10.5047/w-pass.a01.005, 2014.
Tian, H. Z., Zhu, C. Y., Gao, J. J., Cheng, K., Hao, J. M., Wang, K., Hua, S. B., Wang, Y., and Zhou, J. R.: Quantitative assessment of atmospheric emissions of toxic heavy metals

from anthropogenic sources in China: historical trend, spatial distribution, uncertainties, and control policies, Atmos. Chem. Phys., 15, 10127-10147, doi:10.5194/acp-15-10127-2015, 2015.

Tóth, Á., Hoffer, A., Pósfai, M., Ajtai, T., Kónya, Z., Blazsó, M., Czégény, Z., Kiss, G., Bozóki, Z., and Gelesér, A.: Chemical characterization of laboratory-generated tar ball particles, Atmos. Chem. Phys., 18, 10407-10418, doi.org/10.5194/acp-18-10407-2018, 2018.

Vekeman, B., Janssens, K., Vincze, L., Adams, F., and Epsen, P. V.: Analysis of X-ray spectra by iterative least squares (AXIL): New developments, X-ray Spectrompetry, 23(6), 278-285, 10.1002/xrs.1300230609, 1994.

Wu, L., Li, X., Kim, H., Geng, H., Godoi, R. H. M., Barbosa, C. G. G., Godoi, A. F. L., Yamamoto, C. I., de Souza, R. A. F., Pöhlker, C., Andreae, M. O., and Ro, C. U.: Single-particle characterization of aerosols collected at a remote site in the Amazonian rainforest and an urban site in Manaus, Brazil, Atmos. Chem. Phys., 19, 1221–1240, https://doi.org/10.5194/acp-19-1221-2019, 2019.

Wu, L., Becote, C., Sobanska, S., Flaud, P.-M., Perraudin, E., Villenave, E., Song, Y.-C., and Ro, C.-U.: Hygroscopic behavior of aerosols generated from solutions of 3-methyl-1,2,3-butanetricarboxylic acid, its sodium salts, and its mixtures with NaCl, Atmos. Chem. Phys., 20, 14103–14122, https://doi.org/10.5194/acp-20-14103-2020, 2020.

Xu, M. H., Yan, R., Zheng, C. G., Qiao, Y., Han, J., and Sheng, C. D.: Status of trace element emission in a coal combustion process: a review, Fuel Process. Technol., 85, 215–223, doi:10.1016/S0378-3820(03)00174-7, 2004.

Yan, J., Chen, L., Lin, Q., Li, Z., Chen, H., and Zhao, S.: Chemical characteristics of submicron aerosol particles during a long-lasting haze episode in Xiamen, China, Atmos. Environ., 113, 118-126, 10.1016/j.atmosenv.2015.05.003, 2015.

Yu, Z., Zhang, M., Kim, S., Bae, C., Koo, B., Beardsley, R., Park, J., Chang, L. S., Lee, H. C., Lim, Y.-K., and Cho, J. H.: Simulating the impact of long-range-transported Asian mineral dust on the formation of sulfate and nitrate during the KORUS-AQ Campaign, ACS Earth Space Chem., 4, 1039-1049, https://dx.doi.org/10.1021/acsearthspacechem.0c00074, 2020.

Zhang, J., Wang, Y., Teng, X., Liu, L., Xu, Y., Ren, L., Shi, Z., Zhang, Y., Jiang, J., Liu, D., Hu, M., Shao, L., Chen, J., Martin, S.T., Zhang, X., Li, W.: Liquid-liquid phase separation reduces radiative absorption by aged black carbon aerosols. Commun. Earth Environ., 3(1), 128, https://doi.org/10.1038/s43247-022-00462-1, 2022.

Zhang, R., Khalizov, A. F., Pagels, J., Zhang, D., Xue, H., and McMurry, P. H.: Variability in morphology, hygroscopicity, and optical properties of soot aerosols during atmospheric processing, Proc. Natl. Acad. Sci. U.S.A, 105(30), 10291-10296, doi/10.1073/pnas.0804860105, 2008.

Supporting Information

Physicochemical and Temporal Characteristics of Individual Atmospheric Aerosol Particles in Urban Seoul during KORUS-AQ Campaign: Insights from Single-Particle Analysis

Hanjin Yoo[1,2], Li Wu[3], Hong Geng[4,+], and Chul-Un Ro[1,2,+]

[1] Department of Chemistry, Inha University, Incheon, 22201, Republic of Korea

[2] Particle Pollution Management Center, Inha University, Incheon, 21999, Republic of Korea

[3] School of Earth Science System, Tianjin University, Tianjin, China

[4] Institute of Environmental Science, Shanxi University, Taiyuan, China

Correspondence to: Chul-Un Ro (curo@inha.ac.kr) and Hong Geng (genghong@sxu.edu.cn)

A summary of the supporting information:

Figure S1
Section A. Classification of individual particle types
Table S1
Figures S2-S4

Figure S1. Google map of the sampling site. (Map Copyright © Google Earth)

Section A. Classification of individual particle types

The chemical species of individual aerosol particles were determined based on their characteristic morphology and elemental compositions, as detailed in Table S1 and supported by our previous studies (Geng et al., 2011a; 2014). The method for classifying the chemical species of individual aerosol particles is as follows: firstly, particles with an atomic fraction of a chemical species above 90% were considered as a single chemical species. Secondly, reacted and internally mixed particles were identified based on all chemical species and morphology. Thirdly, elements with a concentration of less than 1% were disregarded for the classification, except for N and S (0.5%) which indicate the presence of nitrate and sulfate, respectively. More detailed description of particle type classification based on elemental compositions, morphology, and possible sources can be found in Table S1. In total, 8004 individual particles from 52 samples collected during 5/23-6/5, 2016 (excluding 5/24 due to rain) were classified into seven major types: genuine and reacted mineral dust; reacted sea-spray aerosols (SSAs) and a mixture of SSA and others; secondary aerosol particles (including secondary organic aerosols (SOAs) and secondary organic and inorganic aerosols (SOIAs)); Fe-rich particles; heavy metal-containing particles; particles from combustion events such as soot, tar balls, fly ash, and char particles; and biogenic and humic-like substances (HULIS) particles.

Table S1. Characteristic morphologies and chemical compositions and possible sources of individual particle types

Particle types		Characteristic morphologies and chemical compositions	Possible sources
Genuine mineral dust		Irregular-shaped and bright on their secondary electron image (SEI), including aluminosilicates (mainly containing Al, Si, and O), SiO_2, $CaCO_3$, $CaMgCO_3$, TiO_2, etc.	Soil, mining, and construction sites
Reacted mineral dust		Irregular-shaped particles often surrounded by liquid droplet shade Mineral dust particles with N or S (>0.5%).	Reactions of mineral dust with airborne NO_x/SO_2 and/or $(NH_4)_2SO_4$/NH_4NO_3
Reacted sea-spray aerosols (SSAs)		Liquid droplets or/with irregular shape solids containing N or S along with Na, Mg, and Cl.	Reactions of SSAs with NO_x/SO_2 and/or $(NH_4)_2SO_4$/ NH_4NO_3
Secondary aerosols	Secondary organic aerosols (SOAs)	Dark liquid droplets, in which the sum of C and O is more than 90% and the contents of C and O are comparable.	Accumulation and condensation of semi-volatile organic compounds.
	Secondary organic and inorganic aerosols (SOIAs)	Liquid droplets or solid particles in bright angular shape, mostly containing C, O, S and sometimes with N	Mixing of $(NH_4)_2SO_4$/NH_4NO_3 with organic carbons
Fe-rich particles		Bright irregular particles with Fe content of more than 20%	Metallurgical industries, mining, etc.
Heavy metal-containing particles		Particles containing heavy metal elements, i.e., Zn, Ba, Cu, Mn, Pb, Co, V, etc., of elemental concentrations greater than 1%.	Vehicle emissions, tire and brake pad, metallurgical industries, etc.
Particles from combustion events	Soot aggregates	Fractal-like structure on SEI, with more than 90% of C and O	Soot: Combustions Tar ball: smoldering combustion, such as biomass burning Fly ash: Thermal power and industrial plants Char particles: coal combustions
	Tar balls	Bright and round spherules with high contents of C and O	
	Fly ash	Bright and round spherules with high contents of Al, Si, and O	
	Char particles	Bright and irregular morphology with more than 90% of C and O (C is 3 times higher than O in atomic concentration)	
Biogenic and HULIS	Humic-like substances (HULIS)	Mainly containing comparable C and O, sometimes with S. Bright and irregular on SEI	from soil humic organics
	Biogenic	Unique morphology containing typically N and/or P	from ocean or forest emission or plant debris

Figure S2. Morphology, X-ray spectra, and elemental compositions of biogenic particles: (a) fungal spore, (b) microorganism, and (c) trichome or leaf fragment.

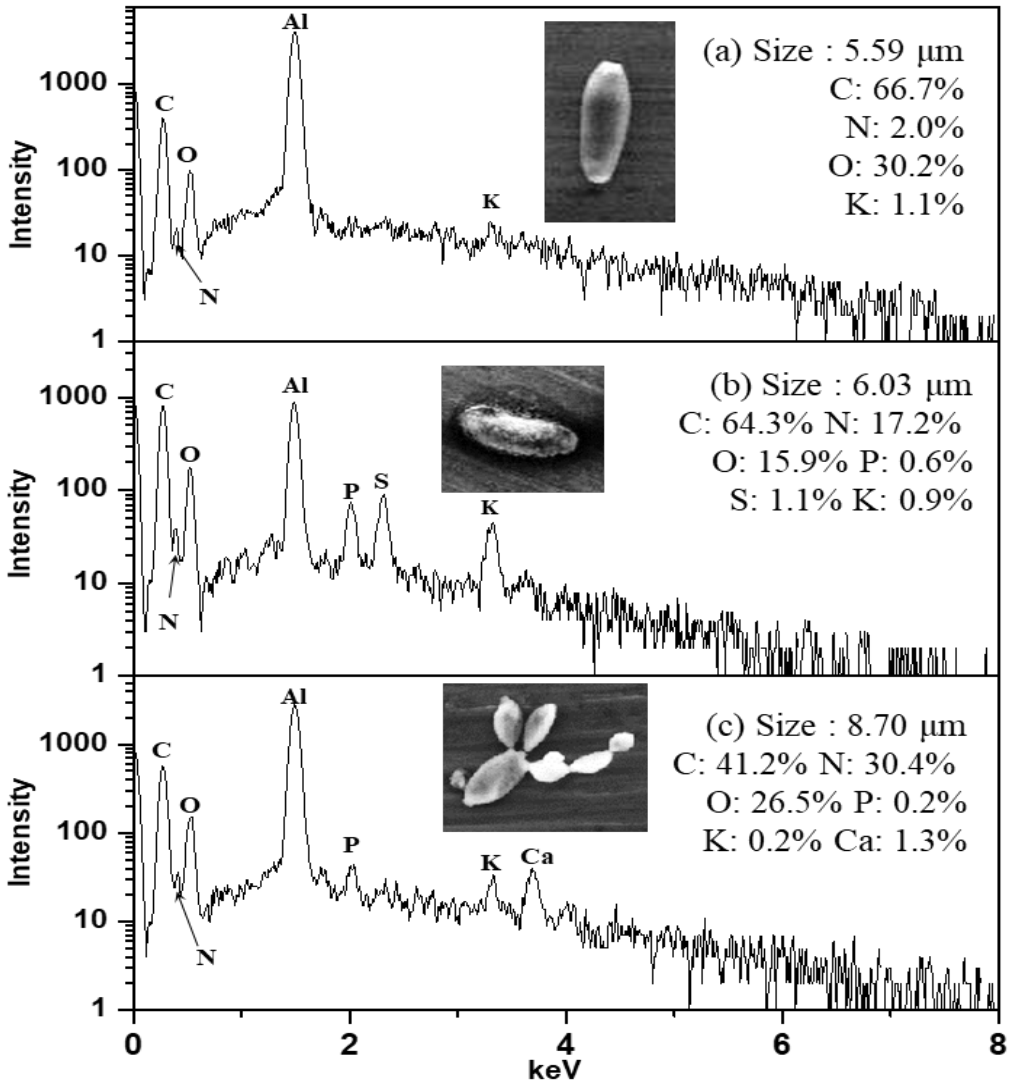

Figure S3. Hourly values of PM_{10} and $PM_{2.5}$ concentrations recorded in Olympic Park, Seoul, during 5/23-6/5, 2016. The blue dots are the sampling times for single-particle EPMA analysis. Black line: PM_{10}; red line: $PM_{2.5}$.

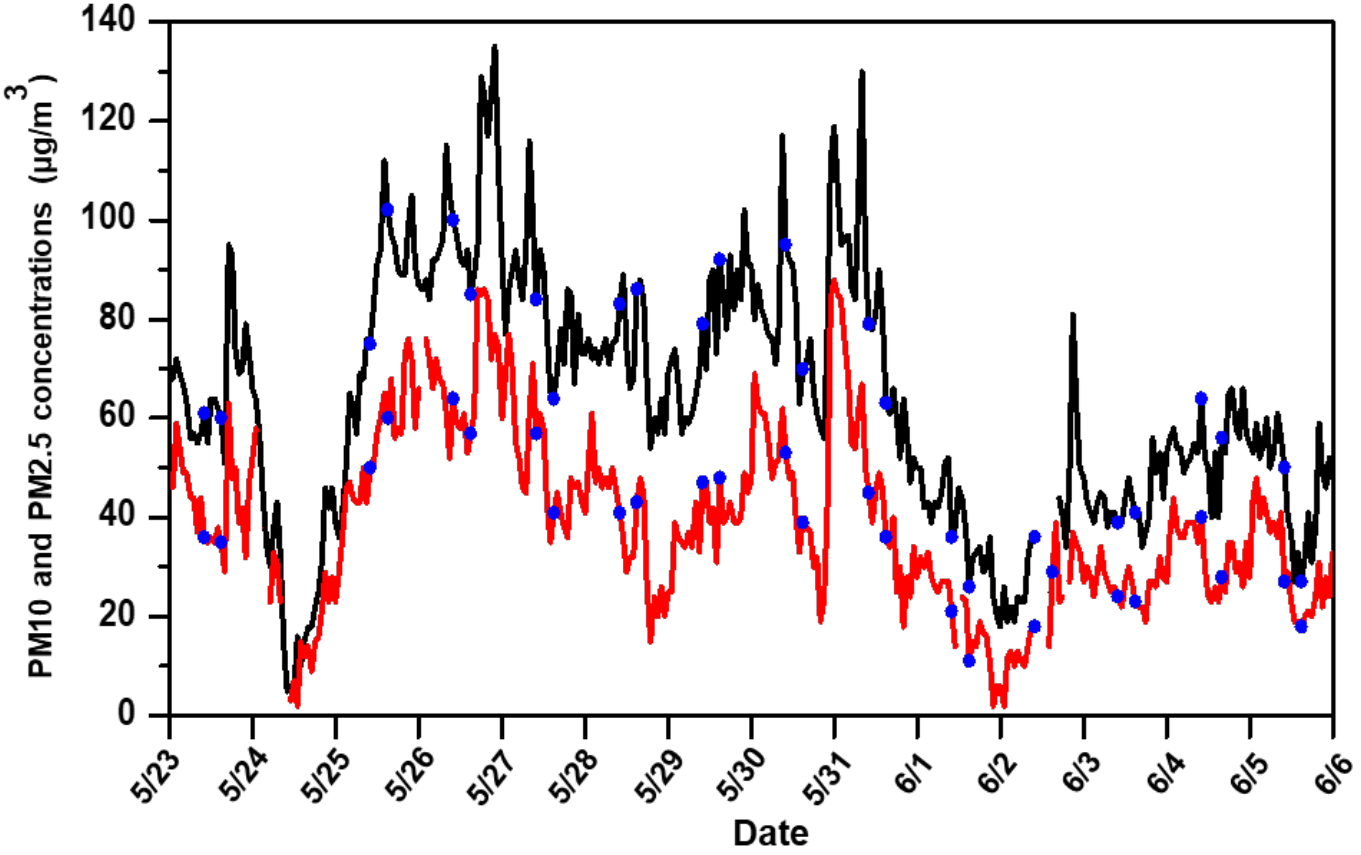

Figure S4. Typical 72-h backward trajectories at 3 different receptor heights (250, 500, and 1000 m above ground level) for (a) 5/23, (b) 5/25, (c) 5/29, (d) 5/30, (e) 6/1, and (f) 6/4.